Biomacromolecules

ARTICLE

pubs.acs.org/Biomac

Gradients with Depth in Electrospun Fibrous Scaffolds for Directed Cell Behavior

Harini G. Sundararaghavan and Jason A. Burdick*

Department of Bioengineering, University of Pennsylvania, Philadelphia, Pennsylvania 19104, United States

ABSTRACT: A major obstacle in creating viable tissue-engineered constructs using electrospinning is the lack of complete cellularization and vascularization due to the limited porosity in these densely packed fibrous scaffolds. One potential approach to circumvent this issue is the use of various gradients of chemical and biophysical cues to drive the infiltration of cells into these structures. Toward this goal, this study focused on creating durotactic (mechanical) and haptotactic (adhesive) gradients through the thickness of electrospun hyaluronic acid (HA) scaffolds using a unique, yet simple, modification of common electrospinning protocols. Specifically, both mechanical (via cross-linking: ranging from 27−100% modified methacrylated HA, MeHA) and adhesive (via inclusion of the adhesive peptide RGD: 0−3 mM RGD) gradients were each fabricated by mixing two solutions (one ramping up, one ramping down) prior to electrospinning and fiber collection. Gradient formation was verified by fluorescence microscopy, FTIR, atomic force microscopy, and cellular morphology assessment of scaffolds at different points of collection (i.e., with scaffold thickness). To test further the functionality of gradient scaffolds, chick aortic arch explants were cultured on adhesive gradient scaffolds for 7 days, and low RGD-high RGD gradient scaffolds showed significantly greater cell infiltration compared with high RGD−low RGD gradients and uniform high RGD or uniform low RGD control scaffolds. In addition to enhanced infiltration, this approach could be used to fabricate graded tissue structures, such as those that occur at interfaces.

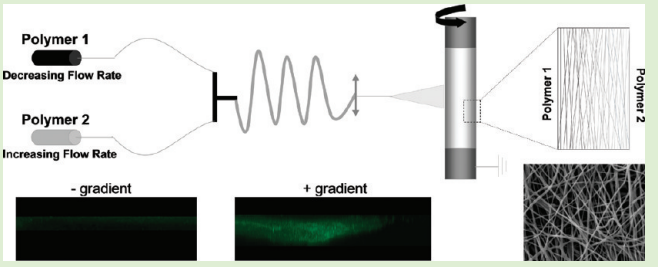

INTRODUCTION

Electrospinning has emerged as a versatile, facile way to develop in vivo-like fibrous scaffolds of synthetic and natural materials, with the ability to control material properties (mechanics, adhesion, degradation) independent of fiber size and orientation.[1−5] Although many studies have investigated electrospun scaffolds for a range of tissue engineering applications, few approaches have been successful in creating clinically viable materials that permit cell integration and infiltration. Often, cellular population and tissue formation occur only at the scaffold periphery.[6] Methods that have been previously used to increase cell infiltration include spinning mixed populations of micro and nano-sized fibers,[7] electrospinning in the presence of cells,[8] spinning with sacrifical fibers,[9] including poragens during fiber collection,[9] and photopatterning,[10] all of which have shown some degree of success in increasing initial cell infiltration into the scaffold. However, these methods typically focus on initial scaffold porosity and do not actually direct cells into the scaffold, which can be very important for scaffold integration and vascularization.

Directed cell migration is critical during many physiological processes such as tissue development, tumorigenesis, and wound healing and has potential use in several tissue engineering applications, such as tissue vascularization, neurite alignment, and constructs for tissue interfaces. Common approaches to direct cells include gradients of mechanics, adhesion and growth factors, and physically through aligned channels and fibers.[11−16] Although growth factors are generally the most influential on cell migration, they are difficult to integrate into tissue engineered scaffolds because both a source and sink for the molecules are necessary.[17,18] Mechanical and adhesive gradients can potentially be included into tissue-engineered constructs, yet the majority of work in this area has been in two dimensions because gradients are difficult to incorporate into 3D scaffolds. Some 3D examples include chemical gradients in agarose,[18] polyethylene glycol (PEG)[19] and collagen[11,20] hydrogels, and mechanical gradients in collagen[11] and PEG[19] hydrogels by modulating cross-linking density. Yet, gradients in fibrous systems have been limited. In fibrous electrospun systems, gradients of materials have been shown in the $x-y$ direction,[3] and gradients of nanoparticles[21] have been previously fabricated, but these systems have been limited in their ability to control cell behavior with scaffold depth, including infiltration.

Thus, there is a need for systems that can direct cell migration while harnessing the benefits of ECM-like fibrous scaffolds. We have chosen to use hyaluronic acid (HA) for this study because of our ability to manipulate mechanics, adhesion, and degradation within HA gels.[22−24] HA is a naturally found nonadhesive, biocompatible polysaccharide that is made up of alternating D-glucuronic acid and *N*-acetyl-D-glucosamine and is found in most connective tissues and has been previously used for applications such as bone[25] and neural tissue engineering.[26] HA can be

Received: March 26, 2011
Revised: April 29, 2011
Published: May 02, 2011

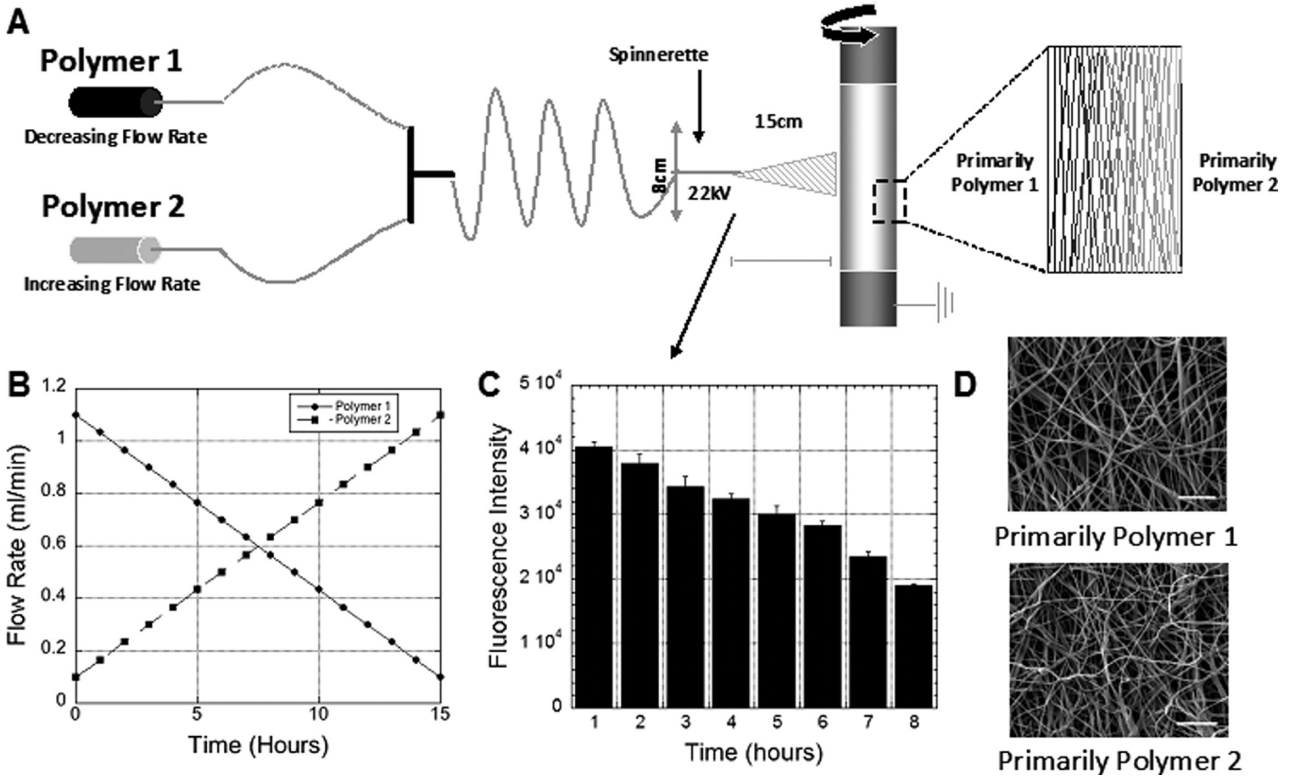

Figure 1. (A) Schematic of electrospinning apparatus. Gradients were created in the *z* direction (scaffold depth) by modulating flow rates of Polymer 1 and Polymer 2, which were mixed prior to the spinnerette and electrospinning. (B) Change in pump flow rate with time for Polymer 1 and Polymer 2. (C) Electrospinning solution (Polymer 1 solution contained a fluorescent dye, whereas Polymer 2 solution did not) was collected from the spinnerette every hour for 8 h, prior to electrospinning, and the fluorescence was measured as shown. A decrease in fluorescence intensity with time verifies the potential gradient formation at the spinnerette and therefore potential gradient formation in the electrospun mat. (D) SEM micrographs show similar fiber morphology on the top and bottom of an electrospun gradient scaffold (scale bar = 10 μm).

readily modified on its hydroxyl group with methacrylation and photo-cross-linked to form a hydrogel.[23] Varying the extent of methacrylation can be used to control the mechanical and degradation characteristics of these hydrogels,[23,27] whereas the coupling of adhesive peptides (e.g., RGD) can also be used to alter cellular interactions.[28] The electrospinning of HA is one approach to create soft, yet fibrous scaffolds for tissue engineering applications,[10,29−31] and the porosity of HA electrospun scaffolds can be controlled either through patterning,[10] electrospinning with sacrificial fibers,[9] or controlling the degradability of the HA networks.[24]

Herein, we present a unique method to create depth-wise mechanical and adhesive gradients through the thickness of HA-based electrospun scaffolds. This was accomplished by modulating the flow rate of two programmable syringe pumps, each with distinct precursor solutions, one increasing speed and one decreasing speed, to change the concentration of a fluorescent molecule or either methacrylation percentage or amount of adhesive peptide on the HA backbone during scaffold collection.

MATERIALS AND METHODS

Macromer Synthesis. Methacrylated HA (MeHA) was synthesized by reacting methacrylic anhydride (20-fold excess, Sigma) with a 1 wt % sodium hyaluronate (MW 66 kDa, Lifecore, Chaska, MN) in DI H_2O solution adjusted to pH 8 with 5N NaOH on ice for 24 h, as previously described.[23] After reaction, the polymer was purified by dialysis against water for 48 h and then lyophilized to produce the final product. The percent methacrylation (number of repeat units containing a macromer) was adjusted based on the amount of methacrylic anhydride added to the reaction and was determined to be ~27, ~30, or ~100% with ^{1}H NMR (Bruker Advance 360 MHz, Bruker, Billerica, MA) for this study. To promote cell adhesion, MeHA was modified with adhesive peptides through the addition reaction of an RGD peptide with a free thiol group (GCGYG**RGD**SPG, Genscript, Piscataway, NJ) with the methacrylate groups for a final theoretical concentration of 0, 1, or 3 mM RGD in the samples. Specifically, RGD peptide and MeHA were coupled by reacting overnight in triethanolamine buffer, dialyzing against DI H_2O for 48 h, and lyophilizing to obtain MeHA-RGD.[10]

Electrospinning HA Scaffolds. MeHA (2 wt %) was cospun with polyethylene oxide (PEO, 3 wt %, MW 900 kDa, Sigma), as previously described.[4,10] The polymer solution (HA, PEO, and 0.05 wt % Irgacure 2959 (I2959, Ciba) photoinitiator in water) was ejected at 1.2 mL/h using a syringe pump (KD Scientific, Holliston, MA) through a 12 cm long, 18 gauge needle charged to 22 kV onto a custom built rotating mandrel (2 in. diameter aluminum, ~5 m/s, ~1800 rpm) at a distance of 15 cm for 15 h. The rotation speed of the mandrel was designed to collect fibers in a random orientation, rather than aligned. To view fiber morphology, scaffolds were imaged using scanning electron microscopy (SEM, JEOL 7500F HRSEM, Penn Regional Nanotechnology Facility). After collection, scaffolds were removed from the mandrel to create a rectangular mat (18 × 15 cm, ~500 μm thick), cross-linked with 10 mW/cm^2 UV light exposure under nitrogen for 30 min and immersed in PBS for 24 h to swell and equilibrate (rinsing three times).

Gradient Formation. Depth-wise gradients were produced using the above electrospinning approach, except that two syringe pumps

(200P, KD Scientific) programmed to change pumping velocity over a specified time range were used to introduce the electrospinning solution. (See the schematic in Figure 1) In this arrangement, solutions meet at a t-junction, go through a mixing channel, and are ejected through the electrospinning needle (i.e., spinnerette) at a constant rate of 1.2 mL/h. For gradient scaffolds, two different polymer solutions were used (polymer solutions used depend on gradient formed) where the flow rate of Polymer 1 ranged from 1.1 to 0.1 mL/h (decreasing 0.067 mL/h each hour) and the flow rate of Polymer 2 ranged from 0.1 to 1.1 mL/h (increasing 0.067 mL/h each hour) (Figure 1B). Thus, the final scaffold is collected as primarily Polymer 1 at the bottom (the side of the scaffold against the mandrel) and primarily Polymer 2 at the surface.

Gradient Verification. Gradients were verified using several techniques. Initially, the formation of a gradient in the solution prior to electrospinning was verified by the addition of a fluorescein dye to only the Polymer 1 solution and the collection of the electrospinning solution every hour for 8 h. A change in fluorescent dye concentration was measured with a fluorescence plate reader (Tecan, Durham, NC). Gradient formation in the fibrous scaffolds was verified during the electrospinning process by collecting fiber samples from the collection mandrel every hour for 15 h. Methacrylated rhodamine (MeRho, Polysciences, Warrington, PA) was added at a concentration of 25 μM to Polymer 1 solution (30% MeHA modification, no RGD) to incorporate fluorescence into the fibers, whereas Polymer 2 had the same solution without MeRho. Every hour, three methacrylated glass coverslips (22 mm ×22 mm) were secured to the mandrel during electrospinning with tape. The coverslips were removed and cross-linked with 10 mW/cm^2 UV light, and their fluorescence was evaluated (five images/sample) using a Zeiss HBO 100 (Thornwood, New York) inverted fluorescent microscope and the "mean gray value" tool on Image J (NIH, v1.42). These samples were also assessed with attenuated total reflectance Fourier transform infrared spectroscopy (ATR-FTIR, Nicolet 6700, Thermo Fisher Scientific, Waltham, MA, 256 scans). Specifically, the area under the aromatic peak in rhodamine (1500−1700) was compared with the area under the methylene peak (2800−3000) present in HA, which remains constant.

Mechanical Gradients. Mechanical gradient scaffolds were fabricated by altering polymer cross-linking with depth through the extent of HA methacrylation in each solution: Polymer 1 was a solution of 27% modified MeHA, 1 mM RGD and Polymer 2 was a solution of 100% modified MeHA, 1 mM RGD. Both solutions contained MeRho (25 μM) to visualize fibers. Every 2 h for 16 h during electrospinning, three methacrylated glass coverslips (22 mm × 22 mm) were secured to the mandrel for sample collection, which were subsequently cross-linked and equilibrated in PBS. Confocal images of fiber samples were taken at 60× (Zeiss Axiovert 100, Thornwood, New York), and fiber diameter was measured using Image J (NIH, v1.42). Atomic force microscopy (AFM) was used to examine the local mechanical compliance of electrospun HA scaffolds. Force measurements (30 measurements were made on three samples/condition and performed in water to eliminate capillary effects) were taken with an Asylum Research AFM (Santa Barbara, CA) in the small force regime (cantilever stiffness ∼0.06 N/m, 25 μm spherical radius polystyrene probe, Novascan Technologies, Ames, IA). Displacement was measured by a linear variable differential transformer (LVDT) sensor, and elastic moduli were obtained by fitting force−indentation graphs to a Hertz model, as previously described.[32] Fiber morphology and scaffold porosity is not affected by cross-linking, as previously shown.[10]

Adhesive Gradients. Adhesive gradient scaffolds were fabricated by altering HA-RGD concentration in each solution: Polymer 1 was a solution of 30% modified MeHA, 3 mM RGD and Polymer 2 was a solution of 30% modified MeHA, 0 mM RGD. Every 2 h for 16 h, three methacrylated glass coverslips (22 mm ×22 mm) were secured to the mandrel for sample collection, which were subsequently cross-linked, equilibrated in PBS, and sterilized with germicidal lamp exposure. Human umbilical vein endothelial cells (HUVECs, Lonza, Walkersville, MD) were plated on scaffolds at a concentration of 9×10^3 cells/mL (3 mL/well) for 24 h, fixed in 4% formalin for 30 min, washed three times for 5 min in wash buffer (1% BSA, 0.5% Triton-X), and incubated in fluorescein isothiocyanate (FITC) phalloidin (0.66 mg/mL, Invitrogen, Carlsbad, CA) to visualize. Cells were imaged using a Zeiss HBO 100 (Thornwood, New York) inverted fluorescence microscope, and the cell spread area was measured using Image J (NIH, v1.42) for all cells observed in five images/sample and three samples/time point of collection.

Aortic Arch Culture. Chick aortas were isolated from 12-day-old chick embryos (Charles River Laboratories, Preston, CT). Aortic arches were cleaned of excess fibroadipose tissue and cut into 1 mm sized pieces. Each explant was placed individually on an electrospun scaffold sample surface and cultured in media (EGM-2, Lonza, Walkersville, MD, changed every three days). Four different conditions were tested in triplicate: low−high adhesion gradient (0−3 mM RGD, surface−bottom), high−low adhesion gradient (3−0 mM RGD, surface−bottom), uniform high RGD control (theoretical RGD concentration of ∼2.8 mM), and uniform low RGD control (theoretical RGD concentration of ∼0.3 mM). After 7 days, samples were fixed in 4% formalin for 30 min, washed three times for 5 min in wash buffer (1% BSA, 0.5% Triton-X), incubated in FITC-phalloidin (0.66 mg/mL, Invitrogen, Carlsbad, CA) to visualize, and imaged with confocal microscopy (Zeiss Axiovert 100, Thornwood, New York). Images were taken through the thickness of the sample at 10 μm sections, and the sample was reconstructed to view the z-direction migration using LSM Image browser (v4.2.0.121). Infiltration area and maximum infiltration depth were measured using Image J (NIH, v1.42).

Statistics. For all experiments, three discrete samples were evaluated, and error bars indicate standard deviation, unless otherwise specified. For fluorescence gradient verification experiments, three separate samples were fabricated, and five images were evaluated per sample. For AFM measurements, three separate samples were evaluated with at least 10 measurements per sample. For cell area experiments, three separate samples were fabricated with five images taken per sample, and all cells in the images were measured. Statistics were assessed by one-way ANOVA with Tukey's HSD posthoc testing, and p values less than 0.05 were considered to be significant. Please note that for all gradient measurements, there was statistical significance between the first and last collections and many of the time points of collection regardless of outcome (fluorescence, swelling, mechanics, cell spreading); however, statistical differences were not observed between all groups along the gradient.

RESULTS AND DISCUSSION

Electrospun scaffolds have been applied to many different tissue systems and have shown great promise in the field of tissue engineering because of their ability to mimic natural fibers, which allow cells to take a natural, spread morphology. However, their prevalence has been hampered because of issues such as limited cell infiltration due to the dense packing of fibers, particularly for fiber-aligned structures where the packing leads to very low porosity. The most common approach that has been used to increase cell infiltration is by increasing the initial pore size through the addition of sacrificial fibers or poragens, spinning of both micro and nanosize fibers, or through photopatterning.[7,9,10] However, there are limitations to these approaches, including compromised mechanics that occur with increased porosity and the lack of these approaches to provide the necessary cues to entice cellular infiltration into the scaffolds. Thus, we felt it would be advantageous to fabricate scaffolds that contained gradients of cues with depth in the scaffold, using techniques compatible with mechanical, chemical, and soluble signals to encourage cell infiltration. Although gradient scaffolds have been used for wound healing, nerve regeneration, and tissue interfaces because

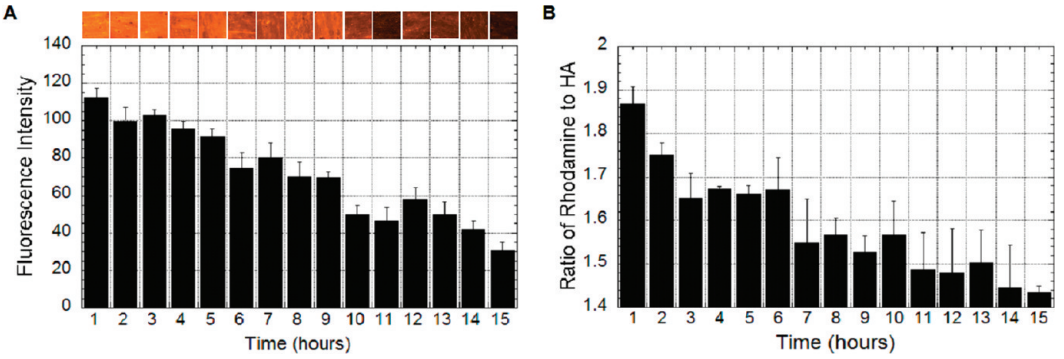

Figure 2. Verification of gradients in fibrous scaffolds. Polymer 1 (30% modification, 25 μM methacrylated rhodamine) contained rhodamine to visualize gradient formation in electrospun scaffolds. Electrospun fiber samples were collected every hour for 15 h to assess changes in rhodamine concentration as the scaffold collects (i.e., initial samples are near sample bottom, whereas later samples are near scaffold surface). (A) Fluorescence intensity (measured by fluorescence microscopy) decreased as the concentration of Polymer 2 (30% modification, no MeRho) increased in the electrospun fibers, further confirming gradient formation. Images showing a decrease in fluorescence intensity with respect to collection time are shown above graph for clarification (n = 3, error bars indicate standard deviation). (B) Using ATR-FTIR, the magnitude of the area under the aromatic peak in rhodamine (1500−1700) normalized to the area under the methylene peak (2800−3000) was observed to decrease with scaffold depth. (n = 3, error bars indicate standard deviation).

of their ability to direct cell growth, much of this work was characterized in only two dimensions, and there does not appear to have been any techniques developed previously for gradients with depth in fibrous scaffolds. One previous study has shown the ability to create gradients of nanoparticles with depth, which can also be potentially incorporated in this system.[21]

Gradient Formation. Thus, a new approach was used to create gradient electrospun scaffolds from HA-based materials, where the flow rate of two solutions is altered over the scaffold collection period. In our design (Figure 1A), Polymer 1 solution was slowly ramped from 1.1 to 0.1 mL/h, and Polymer 2 solution was slowly ramped from 0.1 to 1.1 mL/h, prior to meeting at a mixing t-junction and ejection through a charged needle for electrospinning and collection on a rotating mandrel (Figure 1B). With this notation, the solution collects so that the bottom of the scaffold (region closest to the mandrel) contains a high concentration of the components of Polymer 1 solution, whereas the top of the scaffold contains a high concentration of the components of Polymer 2 solution. The flow rate of the solution through the electrospinning needle remains constant at 1.2 mL/h throughout electrospun scaffold formation, and uniform scaffolds can be fabricated with one pump at this same constant velocity. It should be noted that there is some imperfection in the gradient formation due to the randomness of fiber collection on the mandrel. Fibers may fall at any location throughout the width of the mandrel during gradient formation; however, we have used several methods to verify gradient formation throughout the thickness of the scaffold. Gradient formation was observed by adding a fluorescent dye to only the Polymer 1 solution and collecting the electrospinning solution from the spinnerette prior to fiber formation. A decrease in the concentration of the dye was observed with time, indicating a transition from the solution of Polymer 1 to the solution of Polymer 2 (Figure 1C). Also, the top and bottom of the scaffold was visualized with SEM to verify fiber formation and uniformity throughout the scaffold (Figure 1D).

The ability to obtain gradients in the scaffolds was further verified by creating a fluorescent gradient scaffold where Polymer 1 solution contained MeRho (to visualize individual fibers, 25 μM) and Polymer 2 solution did not. After collection, the samples were then cross-linked using a light-initiated radical polymerization, and the samples were swollen to equilibrium. We expect both inter- and intrafibrous cross-links to occur during the polymerization process; interfibrous cross-links provide stability to the fibers, and intrafibrous cross-links are necessary for a cohesive scaffold. Fluorescence microscopy images and quantification of the samples collected every hour during scaffold formation are shown in Figure 2A, and a clear trend of a decrease in fluorescence is observed with time, indicating more fluorescence at the scaffold bottom than the scaffold surface. Fluorescence intensity measurements are strongly affected by the density of fibers, which may explain some fluctuations in fluorescence measurements. Quantification of FTIR measurements of these same samples indicates a trend of decreasing rhodamine with time (Figure 2B), further verifying gradient formation. FTIR was not sensitive enough to measure RGD or methacrylation changes directly; therefore, we chose to use methacrylated rhodamine to measure gradient formation indirectly.

Mechanical Gradients. Mechanical gradients were created by electrospinning two different modifications of HA (27 and 100% modified MeHA). Higher modification HA has more methacrylates on the backbone and can therefore create more cross-links, which leads to an increased modulus (measured with AFM) and decreased swelling (measured with confocal microscopy due to MeRho incorporation). Previous work has shown the ability to change the compressive mechanics, swelling behavior of MeHA gels, and the tensile properties of MeHA fibrous scaffolds through the number of methacrylates on the MeHA backbone.[10,23] The diameter of swollen fibers showed a general trend of decreasing with time (Figure 3A) from 0.94 ± 0.02 to 0.60 ± 0.02 μm, implying a decrease in fiber swelling with increasing methacrylation from the bottom to the top of the scaffold, as expected. No visual nonuniformity was observed in the swollen fibrous scaffolds. Confocal images show that fiber morphology throughout collection remains smooth; however, some aggregation of the MeRho dye is observed in fiber images. When tested with AFM, an increase in the elastic modulus of the fibers was observed with collection time (Figure 3B), confirming the formation of a mechanical gradient with scaffold thickness. The mechanical gradient with these compositions was

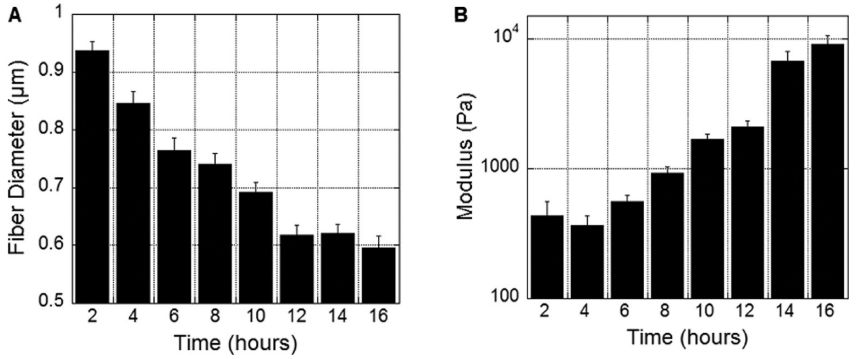

Figure 3. Gradients of mechanics with scaffold depth. Scaffolds with a gradient of mechanics (cross-linking density) were created by electrospinning low-mod MeHA (27% modification, Polymer 1) and high-mod MeHA (100% modification, Polymer 2). Samples were collected every 2 h for 16 h. (A) Methacrylated rhodamine was added to both low- and high-mod MeHA solutions to visualize fibers. Fiber diameter decreased with increasing concentration of high-mod MeHA (scale bar = 20 μm), which correlated to a decrease in swelling of the more cross-linked fibers. (B) AFM measurements show an increase in modulus with increasing concentration of high-mod MeHA (n = 3, error bars indicate standard error).

~0.8 Pa/μm and increased from the bottom to the top of the scaffold.

Mechanical properties of tissue-engineered constructs are emerging as a critical cue for dictating cell behavior including motility and morphology. Several studies have shown the ability of 2D mechanical gradients to direct various cell types including fibroblasts,[12] macrophages,[33] and smooth muscle cells[34] with gradient slopes ranging from 0.2 to 150 Pa/μm. One study showed the ability of shallow (0.06 Pa/μm) 3D mechanical gradients to direct neurite outgrowth, although this study was limited because the low compliance of gels and gradients of this magnitude may not influence other cell types.[11] Electrospun HA gradients build on this previous work by creating fibrous 3D constructs for directed cell migration. Gradient slopes in this study are ~0.8 Pa/μm, which compares well with gradients used to influence macrophages and is approximately an order of magnitude lower than those used in the smooth muscle cell and fibroblast studies.

Adhesive Gradients. Adhesive gradients (high concentration of RGD in Polymer 1 solution, no RGD in Polymer 2 solution) were also fabricated in HA scaffolds by modulating the incorporation of an adhesive peptide. The cell spread area was assessed on swollen fibrous samples collected with time using HUVECs, which showed a ~70% decrease in general cell spreading (μm^2) with time over a 16 h period, indicating a decrease in RGD concentration because spreading can be correlated to integrin interactions with various ligands (Figure 4). The HUVECs transitioned from a fairly spread cell morphology with extensions on the scaffold surface to a nearly rounded cell morphology with few extensions on fibers with collection time (i.e., from the scaffold bottom to the surface).

For full thickness gradient functionality studies (~1 mm thick when hydrated), chick aortic arch samples were placed on scaffolds (low to high, high to low, uniform low, and uniform high RGD) and cultured for 7 days. Representative confocal images of FITC−phalloidin stained (explants), both from the surface and throughout the scaffold depth, are shown in Figure 5. "Top View" images show enhanced growth in high−low gradients and low−high gradients scaffolds, whereas high uniform scaffolds show inconsistent growth and low uniform scaffolds show stunted growth (Figure 5). "Side View" images show cell infiltration into the thickness of the scaffolds. Significantly

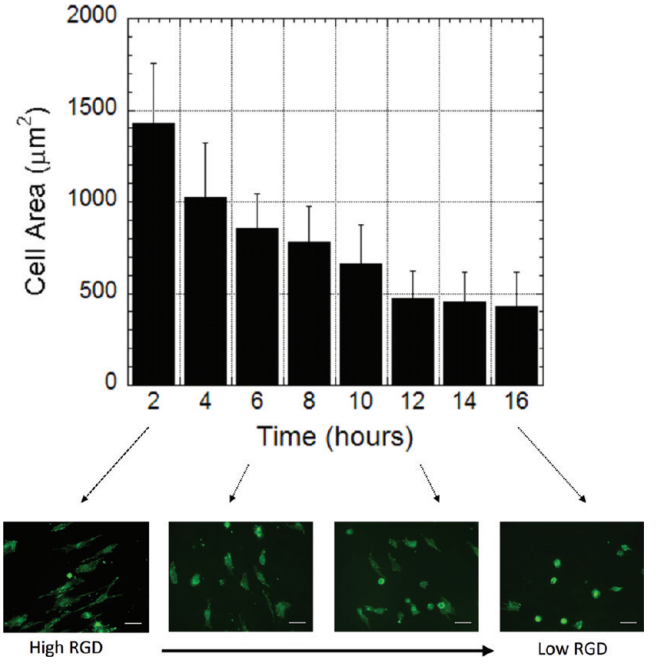

Figure 4. Gradients of adhesion with scaffold depth. Scaffolds with a gradient of adhesion were created by electrospinning high-RGD MeHA (3 mM, Polymer 1) and low-RGD MeHA (0 mM RGD, Polymer 2). Samples were collected every 2 h for 16 h. HUVECs were seeded on swollen scaffolds and cultured for 24 h. A decrease in cell spread area was observed with decreasing RGD (scale bar =50 μm) (n = 3 samples, error bars indicate standard deviation).

increased cell infiltration into the scaffold is observed in the low−high (surface to bottom) gradient scaffolds compared with all other formulations (Figure 6A). Cell infiltration area increased by ~25% compared with high control scaffolds. The maximum infiltration depth, which is defined as the furthest that any cell infiltration has occurred into the scaffold, is significantly greater in uniform high control and low−high gradient control scaffolds (Figure 6B). Uniform high RGD scaffolds showed areas of high infiltration and areas of low infiltration, perhaps due to cell migration on the surface of the scaffold. Because adhesion does not vary between the surface of the scaffold and the thickness of the scaffolds, cells did not show a preference to infiltrate.

However, the infiltration in gradient scaffolds was more consistent through the depth of the scaffold. The maximum infiltration increased from 34 ± 17 μm in the low uniform scaffold to 187 ± 47 μm in the low−high gradient condition.

Adhesive gradients in two dimensions have also been previously shown to have a strong influence on cell behavior including HUVECs,[19] fibroblasts,[13] and smooth muscle cells.[35] Although some work with PEG hydrogels have investigated the ability of gradients to influence cell migration in 3D, for a truly 3D study, cells must migrate through these networks, which has not yet been shown.[19,35] Neurons have been directed through anisotropic agarose networks,[18] although these are not smooth gradients of adhesion. In this work, we have the unique ability to direct cell growth in 3D into fibrous scaffolds. RGD gradients in this study are of the same order of magnitude as previously studied gradients (0.7−5 μM/μm) of adhesion.

Moreover, these current gradients can be modified to include mechanical and adhesive cues that are specific for particular cells to further control cellular behavior. In this study, we chose to verify the functionality of our gradients with a ubiquitous adhesive peptide, RGD;[36] however, this can easily be altered to include alternative peptides and proteins. Additionally, it is possible to test competing gradients in this system to determine which gradients are most influential on cell direction.

HA is a cytocompatible and versatile material that was used in this project. However, this approach is an adaptable technique that can be used with a variety of materials to tailor electrospun scaffolds for specific applications including tissue interfaces, where the scaffold properties and cues can be different on each side of an implant site. Finally, although soluble gradients were not investigated in this study, the release of molecules from the scaffold can also be altered either through loading of different molecule concentrations or through variations in degradation or cross-linking to influence release behavior, to provide a chemotactic cue in the scaffold. Overall, this approach is versatile towards a wide range of applications in tissue engineering.

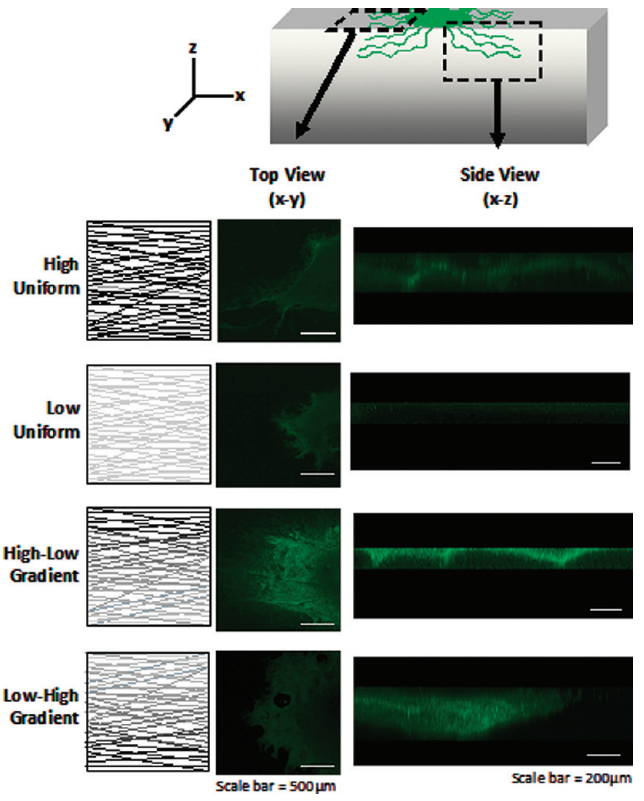

Figure 5. Tissue ingrowth into adhesive gradient scaffolds. Cell infiltration into adhesion gradient scaffolds was assessed by culturing chick aortic arch explants on RGD gradient scaffolds for 7 days. Confocal images were taken through the thickness of the scaffold. "Side View" images show increased infiltration into the low−high gradient scaffolds compared with uniform or high−low gradient scaffolds.

CONCLUSIONS

By modulating the standard electrospinning process, we have developed an approach to create novel gradients of mechanics and adhesion in fibrous HA scaffolds. Mechanical gradients led to changes in the elastic modulus with depth in the sample due to changes in cross-linking, whereas adhesive gradients led to changes in cell spread area with depth due to changes in adhesive ligand concentration. The functionality of gradient scaffolds was confirmed by plating aortic arch explants on scaffolds and observing enhancement in cell infiltration with scaffolds that possessed an increasing gradient in adhesion. Specifically, cell infiltration area increased in low−high adhesive gradient samples when compared with high−low adhesive gradients and controls (uniform high or low adhesion). This method can be translated to other gradients (different peptides or mechanics ranges) and

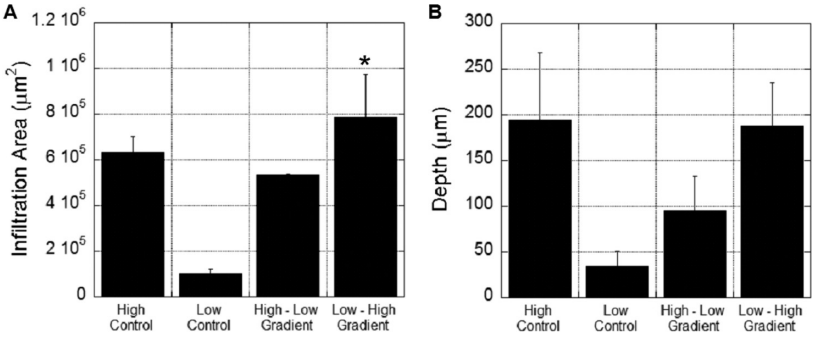

Figure 6. Quantification of cellular growth into gradient scaffolds. (A) Infiltration area (measured with the z-projection of confocal images) showed significantly increased growth in low−high gradient scaffolds ($p < 0.05$) compared with all other conditions. ($n = 3$, error bars indicate standard deviation). (B) Maximum infiltration depth was significantly greater in low−high, high−low, and high uniform control scaffolds compared with low uniform control ($p < 0.05$). However, there was no significant difference in the maximum infiltration depth between high uniform controls and low−high gradient scaffolds ($n = 3$, error bars indicate standard deviation).

to most polymer systems for use in a wide range of tissue engineering applications. Such techniques aim to improve the uniformity of tissues for translational applications or to add complexity for the production of graded tissues.

AUTHOR INFORMATION

Corresponding Author

*E-mail: burdick2@seas.upenn.edu. Tel: 215-898-8537. Fax: 215-573-2071.

ACKNOWLEDGMENT

We would like to acknowledge the experimental assistance of Brandon L. Blakely and Ross A. Marklein. This work was supported by a Fellowship in Science and Engineering from the David and Lucile Packard Foundation and a National Institutes of Health grant R01AR056624.

REFERENCES

(1) Ma, Z.; Kotaki, M.; Inai, R.; Ramakrishna, S. *Tissue Eng.* **2005**, *11*, 101–109.
(2) Pham, Q. P.; Sharma, U.; Mikos, A. G. *Tissue Eng.* **2006**, *12*, 1197–1211.
(3) Baker, B. M.; Handorf, A. M.; Ionescu, L. C.; Li, W. J.; Mauck, R. L. *Expert Rev. Med. Devices* **2009**, *6*, 515–532.
(4) Ifkovits, J. L.; Sundararaghavan, H. G.; Burdick, J. A. *J. Vis. Exp.* **2009**, 32. DOI: 10.3791/1589.
(5) Sill, T. J.; von Recum, H. A. *Biomaterials* **2008**, *29*, 1989–2006.
(6) Baker, B. M.; Mauck, R. L. *Biomaterials* **2007**, *28*, 1967–1977.
(7) Pham, Q. P.; Sharma, U.; Mikos, A. G. *Biomacromolecules* **2006**, *7*, 2796–2805.
(8) Stankus, J. J.; Guan, J.; Fujimoto, K.; Wagner, W. R. *Biomaterials* **2006**, *27*, 735–744.
(9) Baker, B. M.; Gee, A. O.; Metter, R. B.; Nathan, A. S.; Marklein, R. A.; Burdick, J. A.; Mauck, R. L. *Biomaterials* **2008**, *29*, 2348−2358.
(10) Nam, J.; Huang, Y.; Agarwal, S.; Lannutti, J. *Tissue Eng.* **2007**, *13*, 2249–2257.
(11) Sundararaghavan, H. G.; Metter, R. B.; Burdick, J. A. *Macromol. Biosci.* **2010**, *10*, 265–270.
(12) Sundararaghavan, H. G.; Monteiro, G. A.; Firestein, B. L.; Shreiber, D. I. *Biotechnol. Bioeng.* **2009**, *102*, 632–643.
(13) Lo, C. M.; Wang, H. B.; Dembo, M.; Wang, Y. L. *Biophys. J.* **2000**, *79*, 144–152.
(14) Guarnieri, D.; De Capua, A.; Ventre, M.; Borzacchiello, A.; Pedone, C.; Marasco, D.; Ruvo, M.; Netti, P. A. *Acta Biomater.* **2010**, *6*, 2532–2539.
(15) Campbell, D. S.; Regan, A. G.; Lopez, J. S.; Tannahill, D.; Harris, W. A.; Holt, C. E. *J. Neurosci.* **2001**, *21*, 8538–8547.
(16) Hoffman-Kim, D.; Mitchel, J. A.; Bellamkonda, R. V. *Annu. Rev. Biomed. Eng.* **2010**, *12*, 203–231.
(17) Corey, J. M.; Lin, D. Y.; Mycek, K. B.; Chen, Q.; Samuel, S.; Feldman, E. L.; Martin, D. C. *J. Biomed. Mater. Res. A* **2007**, *83*, 636–645.
(18) Kim, S.; Kim, H. J.; Jeon, N. L. *Integr. Biol.* **2010**, *2*, 584–603.
(19) Dodla, M. C.; Bellamkonda, R. V. *Biomaterials* **2008**, *29*, 33–46.
(20) Burdick, J. A.; Khademhosseini, A.; Langer, R. *Langmuir* **2004**, *20*, 5153–5156.
(21) Knapp, D. M.; Helou, E. F.; Tranquillo, R. T. *Exp. Cell Res.* **1999**, *247*, 543–553.
(22) Erisken, C.; Kalyon, D. M.; Wang, H. *Biomaterials* **2008**, *29*, 4065–4073.
(23) Khetan, S.; Burdick, J. A. *Biomaterials* **2010**, *31*, 8228–8234.
(24) Burdick, J. A.; Chung, C.; Jia, X.; Randolph, M. A.; Langer, R. *Biomacromolecules* **2005**, *6*, 386–391.
(25) Sahoo, S.; Chung, C.; Khetan, S.; Burdick, J. A. *Biomacromolecules* **2008**, *9*, 1088–1092.
(26) Chung, C.; Erickson, I. E.; Mauck, R. L.; Burdick, J. A. *Tissue Eng., Part A* **2008**, *14*, 1121–1131.
(27) Wei, Y. T.; Tian, W. M.; Yu, X.; Cui, F. Z.; Hou, S. P.; Xu, Q. Y.; Lee, I. S. *Biomed. Mater.* **2007**, *2*, S142–S146.
(28) Bencherif, S. A.; Srinivasan, A.; Horkay, F.; Hollinger, J. O.; Matyjaszewski, K.; Washburn, N. R. *Biomaterials* **2008**, *29*, 1739–1749.
(29) Marklein, R. A.; Burdick, J. A. *Soft Matter* **2010**, *6*, 136–143.
(30) Ji, Y.; Ghosh, K.; Shu, X. Z.; Li, B.; Sokolov, J. C.; Prestwich, G. D.; Clark, R. A.; Rafailovich, M. H. *Biomaterials* **2006**, *27*, 3782–3792.
(31) Li, J.; He, A.; Zheng, J.; Han, C. C. *Biomacromolecules* **2006**, *7*, 2243–2247.
(32) Yao, C.; Li, X.; Song, T. *J. Biomater. Sci., Polym. Ed.* **2007**, *18*, 731–742.
(33) Dimitriadis, E. K.; Horkay, F.; Maresca, J.; Kachar, B.; Chadwick, R. S. *Biophys. J.* **2002**, *82*, 2798–2810.
(34) Nemir, S.; Hayenga, H. N.; West, J. L. *Biotechnol. Bioeng.* **2009**, *105*, 636–644.
(35) Isenberg, B. C.; Dimilla, P. A.; Walker, M.; Kim, S.; Wong, J. Y. *Biophys. J.* **2009**, *97*, 1313–1322.
(36) DeLong, S. A.; Moon, J. J.; West, J. L. *Biomaterials* **2005**, *26*, 3227–3234.
(37) D'Souza, S. E.; Ginsberg, M. H.; Plow, E. F. *Trends Biochem. Sci.* **1991**, *16*, 246–250 .